LWS Grating Flux Accuracy and Monitoring

Tanya Lim and Martin Burgdorf

31^{th} July 1998

Index

1. Dark Current
1.1 Monitoring Dark Current From Handover Flashes (Martin)
1.2 Dark Current Determination Using A Dedicated Observation (Tanya)
1.3 Dark Current From Parallel Mode (Martin)
2. Responsivity/Flux Obtained
2.1 Monitoring Responsivity From Handover Illuminator Flashes (Martin)
2.2 Flux From Galactic Sources (Tanya)
2.3 Repeatability of Instrument/Pipeline Output
2.4 Consistency Checks With Solar System Objects (Both)
2.4.1 Monitoring of Uranus (Tanya)
2.4.2 Comparison of Mars/Uranus/Neptune with models (Martin)
2.4.3 Comparison of Ceres (only forward scans) with model (Tanya)
2.4.4 Comparison of Ceres (fixed grating position) with model (Martin)
2.4.5 Comparison of Callisto and Ganymede with BB (Martin)
3. Appendix I - Routines Used (Both)
4. Appendix II - Variation in Flux of Galactic Sources

1. Dark Current

Dark current has been largely unchanged throughout the mission. Three different methods have been used to monitor its behaviour and determine its value.

1.1 Monitoring Dark Current From Handover Flashes

Standard illuminator flash sequences using levels 100 and 220 have been performed near the beginning and near the end of every handover window since revolution 150. As part of these sequences the dark current was determined; this provided a dataset uniquely suited for trend analysis, because the measurements were always taken at very similar times within a revolution. The were no illuminator flashes in revolutions 196 and 197 (violation of Earth constraint) and from revolution 378 through 441 (switch-off period).
The program new-lcsi (see appendix) was used to calculate the dark current from the CPD-files. For revolutions 242, 545, 605, 676, 721, 757, 781 and 853 the LCPD-file for at least one of the handover flashes could not be generated; for revolutions 726, 728 and 821 new-lcsi did not terminate successfully.
The remaining values for the dark current are shown in figures 1 - 4. The main result is that the dark currents did not change significantly during the mission except for LW4 and LW5 where they had increased by 30 percent. No systematic drifts were detected within a revolution, either. As tests in the laboratory had shown that ionizing radiation causes a strong rise of both responsivity and dark current, it was a question whether we determined indeed the dark background with our measurements and not a leakage current in the electronic. Therefore a dark current measurement with bias = 0 V was executed; it produced current = 0 A, thus showing that the dark current originated in our detectors. Table 1 gives the mode of the dark current measurements for each detector; the given errors are just the widths of the histogram columns from which the mode was determined. The values here are systematically higher than the ones determined with other methods. The reason for this is that new-lcsi calculates the

median whereas the other methods use only the mode. As the distribution of ramp heights is not quite symmetrical, this means that the median is larger than the mode.

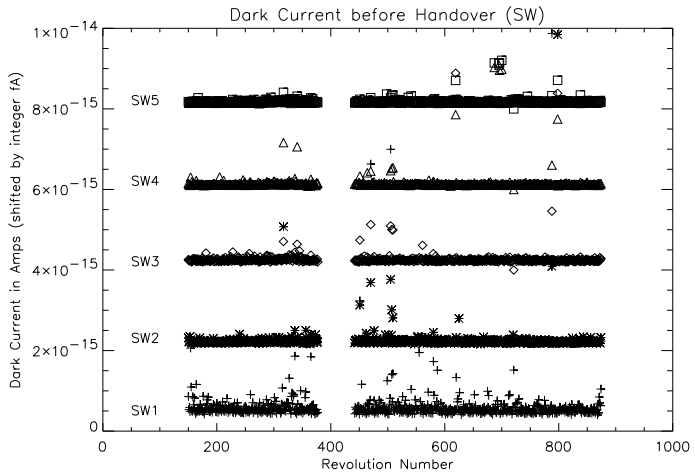

Figure 1: Dark current measurements at handover before bias boost, SW detectors

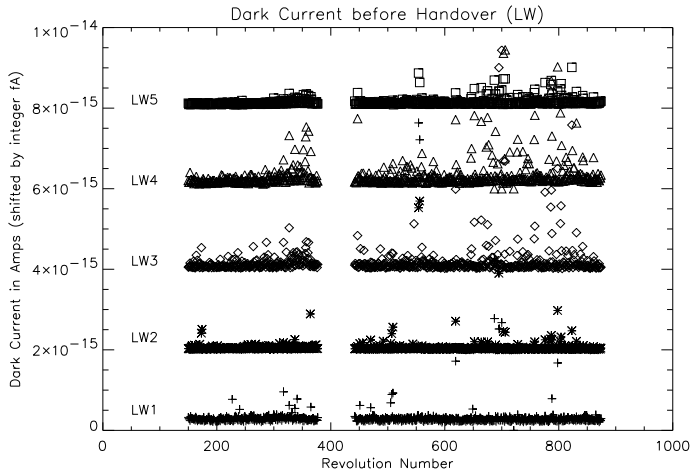

Figure 2: Dark current measurements at handover before bias boost, LW detectors

1.2 Dark Current Determination Using A Dedicated Obsevation

Two one hour measurements of dark current were done in revolution 650 one just after groundstation handover, the other just before the close of the science window. These were done

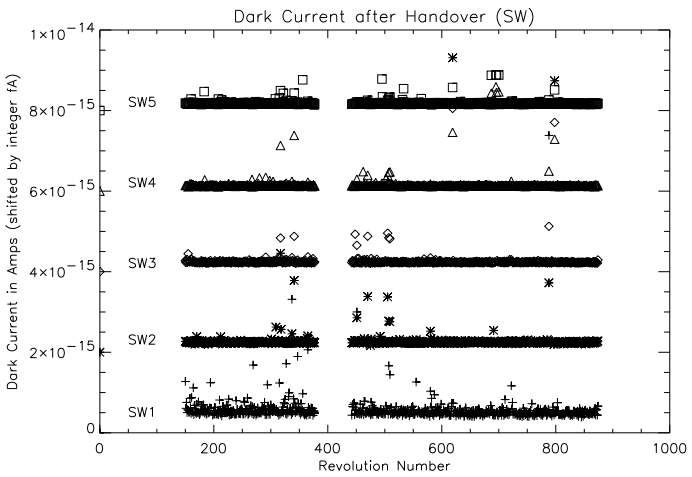

Figure 3: Dark current measurements at handover after bias boost, SW detectors

using a COIF so that the ramp lengths could be varied through the observation. Table 2 gives the time and number of ramps for each observation.

In order to determine the dark current the following procedure was applied for each detector for each ramp length:

1. The mean was found
2. The data were binned into 40 bins from 0 to 2*mean
3. The number of ramps in each bin was plotted as a histogram
4. A gaussian and polynomial were fitted
5. The dark current was determined from the peak of the fitted gaussian

Table 3 gives the detector, multiplication factor then dark currents obtained with each ramp length and part of revolution in Amps. For all detectors except SW1 the dark current was obtained from the position of the maximum of the gaussian fit. For SW1 this was obtained from the maximum of the histogram. It was found that there is no apparent variation in the dark current over the course of the revolution except in two detectors. The results from LW1 indicate that there may be a 10% increase and the results from LW5 indicate there may be a 20% decrease although neither of these is significant. There is no significant difference in dark current measured between 1/4s, 1/2s and 1s ramps.

1.3 Dark Current From Parallel Mode

A third method to determine the dark background uses data from the parallel/serendipity mode. The grating is here in rest position and the ramp length is 1 s. The random pointings of this observing mode have for the most part no significant flux, therefore they provide a huge number of ramps with dark background only. Determining the mode with a method similar to

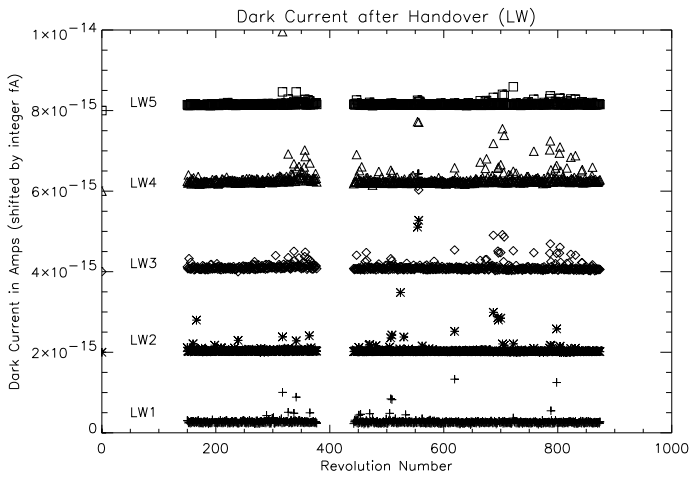

Figure 4: Dark current measurements at handover after bias boost, LW detectors

the one described in the previous chapter gave the results listed in table 1. They are in good agreement with the values derived with dedicated measurements, thus showing that they are not affected by sky background. The errors are here the standard deviations of the Gaussians fitted to the histograms; this explains the difference to the errors in the second column of table 1.

2. Responsivity/Flux Obtained

2.1 Responsivity From Handover Illuminator Flashes

The same illuminator flash sequences during handover that were used for the determination of the dark current served also for monitoring the responsivity of the detectors. We used level 100 for the LW detectors and level 220 for the SW detectors. The results are shown in figures 5 - 8; table 4 shows a comparison between the measured signals from the illuminator flashes at the beginning and the end of the mission. No significant trends were detected, except for a drop in responsivity of detector LW2 by about a third during the switchoff period around revolution 400.
Since the bias boost performed during handover reset the responsivity to the level at the beginning of the revolution, the responsivity values are at the end of the handover window between 0 and 50 percent lower than at the beginning. The standard illuminator flash signal that is used by the pipeline for the photometric calibration gives the responsivities shortly before bias boost.

2.2 Flux From Galactic Sources

Galactic sources such as HII regions are very stable and can be used as an external standard for determining the stability of the detector/illuminator combination over the mission. Essentially the purpose of monitoring galactic sources was to monitor the absolute output of the internal illuminator. Two types of monitoring were done, a check on the output from auto-analysis to check overall calibration stability and repeatability and a check of the output of the illuminators ratioed to the source. Of secondary importance as it was done elsewhere was a check on the dark current and responsivity correction applied.

Detector	Handover	SM
	$10^{-16}Amps$	$10^{-16}Amps$
SW1	4.6 ± 0.1	4.98 ± 0.58
SW2	2.4 ± 0.1	1.98 ± 0.32
SW3	2.2 ± 0.1	2.00 ± 0.23
SW4	1.3 ± 0.1	0.89 ± 0.24
SW5	1.6 ± 0.1	1.35 ± 0.22
LW1	2.5 ± 0.1	2.26 ± 0.30
LW2	0.2 ± 0.1	0.17 ± 0.18
LW3	0.6 ± 0.1	0.39 ± 0.25
LW4	2.2 ± 0.1	1.84 ± 0.33
LW5	1.5 ± 0.1	0.98 ± 0.25

Table 1: Dark Background Determination

Time	Ramp length length	No. Ramps After Handover	No. Ramps End of Revolution
52 minutes	1/2s	6146	6171
2 minutes	1s	236	236
2 minutes	1/4s	927	942

Table 2:

The flux calibration applied in the pipeline is essentially two calibrations, due to two different reference illuminator flashes being used. The changeover occurred during the switch off period between rev 377 and 442. Table 5 gives the number of observations of each of the five main objects in each calibration period.

2.3 Repeatability of Instrument/Pipeline Output

All the observations consist of full grating scans therefore two approaches at monitoring the flux are available. One could use a key wavelength approach i.e. just use the data obtained around say the centre of the detector or the data across the detector could be averaged. The latter approach was adopted. Comparison between the two methods showed very little difference in results i.e. the variation between observations given by the two approaches was similar. The routines to average the data and plot the averages with revolution are described in 3.1.2 and the average flux and sigma of all the observations is given in appendix II.

Det	After Handover 1/4s	End of Revolution 1/4s	After Handover 1/2s	End of Revolution 1/2s	After Handover 1s	End of Revolution 1s
SW1 (*1E-16)	5.18	5.10	4.93	4.99	4.43	4.96
SW2 (*1E-16)	2.36	2.00	2.08	2.08	1.93	2.13
SW3 (*1E-16)	2.07	2.28	2.15	2.25	2.11	2.20
SW4 (*1E-16)	0.88	1.08	1.16	1.20	1.13	1.33
SW5 (*1E-16)	1.55	1.74	1.53	1.58	1.54	1.67
LW1 (*1E-16)	2.37	2.86	2.32	2.67	2.30	2.72
LW2 (*1E-17)	0.98	0.55	0.76	0.70	1.43	0.97
LW3 (*1E-17)	3.46	2.33	5.11	5.51	6.18	4.58
LW4 (*1E-16)	1.86	1.98	1.90	1.61	1.63	1.57
LW5 (*1E-16)	1.08	0.85	1.31	1.11	1.32	1.09

Table 3:

Detector	$I^{150-249}/I_{ref}$	$I^{775-874}/I_{ref}$
SW1	0.9	0.8
SW2	1.0	1.0
SW3	1.0	0.9
SW4	0.9	0.9
SW5	0.9	0.9
LW1	1.1	1.0
LW2	1.2	0.8
LW3	0.9	0.8
LW4	0.9	0.8
LW5	0.8	0.8

Table 4: Change in Performance

2.4 Consistency Checks With Solar System Objects

2.4.1 Monitoring of Uranus

Uranus is essentially the prime calibrator for LWS and is also the object that the flux calibration by use of a standard illuminator flash and RSRF are based on. For the RSRF only one observation of Uranus was used which took place in revolution 317. Therefore all routine L01 observations can be used as an independent check of the RSRF i.e. is the model shape returned? For the flux calibration both the observation in revolution 317 and a subset of the monitoring L01 observations were used in the derivation of the standard flash. The correct application of the flux calibration in the pipeline can therefore be checked using all other Uranus observations.

2.4.2 Comparison of Mars/Uranus/Neptune with models

The slope of the measured grating spectrum of Mars in detectors SW1 and SW2 is different from the models of both Davis and Encrenaz (see figures 9 and 10). A second order polynomial was fitted to the difference between observation and model of Mars and was then added to

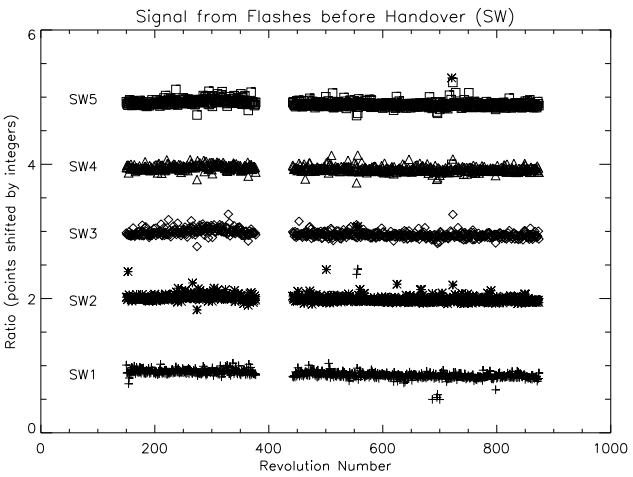

Figure 5: Responsivity checks at handover before bias boost, SW detectors

Object	No. Observations before rev 377	No. Observations after rev 377
S 106	10	28
G 298	11	10
I23133	0	23
NGC 7027	6	20
NGC 6543	36	56

Table 5: Numbers of Observations of the Five Main Galactic Sources

the spectrum of Neptune (see figures 11 and 12). With this correction the spectrum of Neptune agrees in detectors SW1 and SW2 better with the model of Lellouch. Therefore it was a question whether the model of Uranus on which the relative spectral response function is based is correct. Especially at the short wavelength end this model is strongly dependent on assumptions of the planet's temperature profile and less reliable than the predicted continuum flux from Mars. Unfortunately the various spectra taken for monitoring differ at certain wavelengths by up to ten percent. Hence it is difficult to decide to which extent the deviations from the Mars model are caused by changes in the RSRF and to which extent by inaccuracies in the Uranus model.

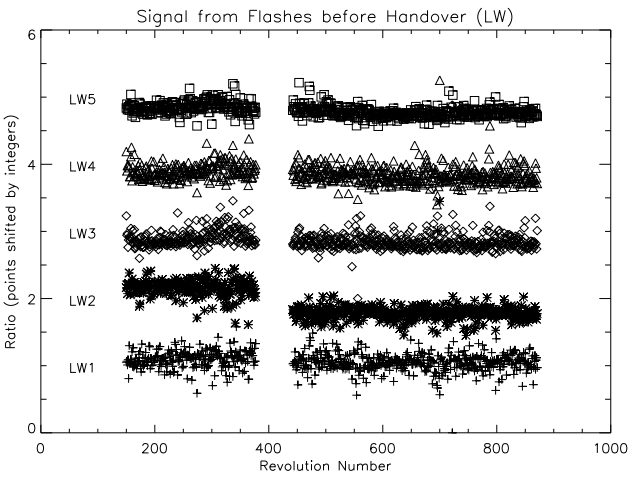

Figure 6: Responsivity checks at handover before bias boost, LW detectors

2.4.3 Comparison of Ceres (only forward scans) with model

A full grating scan AOT was obtained on Ceres during Routine phase which consisted of 20 forward scans only. This observation is problematic not only that it consists only of forward scans but also in that it was affected by straylight thought to be due to the detector block heating up which occurred intermittently in later revolutions. Due to the straylight only the first five detectors can be used for any comparison with the model.

	On-Off	Model	Source/Model
SW1	4.68E-17	5.28E-17	0.89
SW2	2.79E-17	2.71E-17	1.03
SW3	1.83E-17	1.76E-17	1.04
SW4	1.07E-17	1.09E-17	0.98
SW5	7.03E-18	7.21E-18	0.98
LW1	4.80E-18	4.11E-18	1.17
LW2	1.76E-18	2.22E-18	0.79
LW3	1.03E-18	1.12E-18	0.92
LW4	7.82E-19	6.65E-19	1.17
LW5	3.31E-19	4.12E-19	0.80

Table 6: Fluxes from Ceres averaged grating scans with off source subtracted, averaged model fluxes for the equivalent wavelength range and the ratio between them.

2.4.4 Comparison of Ceres (fixed grating position) with model

Ceres is the only asteroid whose lightcurve varies by less than five percent when corrected for its distance from earth, and good models exist of its emission. In order to achieve a high signal to noise ratio most observations on that target were made in the photometric mode of the

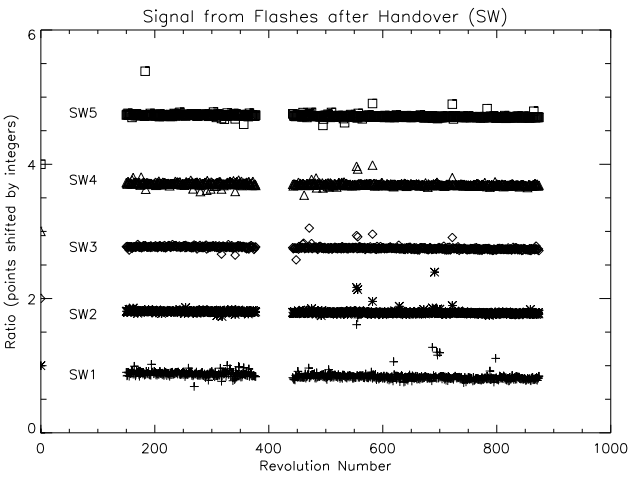

Figure 7: Responsivity checks at handover after bias boost, SW detectors

LWS. The results from the comparison of the measurements with the models (calculated by Th. Mueller) are shown in table 7. The agreement is very good, except for detectors SW1 and LW1. SW1 is known for showing relatively strong memory effects and occasional deviations from the model even for Uranus. There is no explanation, yet, for the too high flux measured with LW1, but it is unlikely that the mistake is caused by an unknown feature in the spectrum that was not included in the model.

Wavelength μm	FD ($\gamma = 0$) Jy		FD ($\gamma = 10$) Jy		FD (STM) Jy		FD (LWS) Jy	
46.1	744	$\pm$37	709	$\pm$35	722	$\pm$36	645	$\pm$21
56.2	576	$\pm$29	552	$\pm$28	560	$\pm$28	526	$\pm$11
66.1	454	$\pm$23	436	$\pm$22	441	$\pm$22	437	$\pm$29
75.7	364	$\pm$18	351	$\pm$18	354	$\pm$18	325	$\pm$19
84.8	297	$\pm$15	287	$\pm$14	288	$\pm$13	288	$\pm$24
102.5	206	$\pm$10	199	$\pm$10	200	$\pm$10	221	$\pm$7
122.2	149	$\pm$7	145	$\pm$7	145	$\pm$6	149	$\pm$10
141.8	112	$\pm$6	109	$\pm$5	109	$\pm$4	101	$\pm$7
160.6	87	$\pm$4	85	$\pm$4	85	$\pm$3	82	$\pm$8
178	78	$\pm$4	76	$\pm$4	76	$\pm$3	63	$\pm$21

Table 7: Ceres in rev. 258

2.4.5 Comparison of Callisto and Ganymede with BB

Figure 13 shows the spectrum of Ganymede. The background was measured right after the

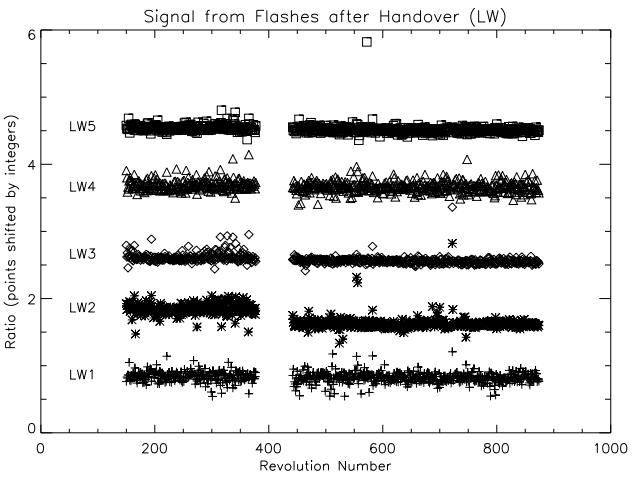

Figure 8: Responsivity checks at handover after bias boost, LW detectors

on-target observation at the same distance from Jupiter (6'). As the straylight depends not only on the distance but also on the direction of the source, the background subtraction was not fully successful. In particular fringes remained and the observed brightness temperature is systematically too low.

Straylight causes less problems for the observations of Callisto. Figure 14 shows its spectrum in brightness temperature; it agrees well with a black body of 145 K up to a wavelength of 100 μm. Also in this case a background measurement at the same distance but different direction from Jupiter was subtracted. Below 50 μm the measured flux from Callisto decreases slightly towards shorter wavelengths. This result is in agreement with what was found for Neptune (see chapter 2.4.2).

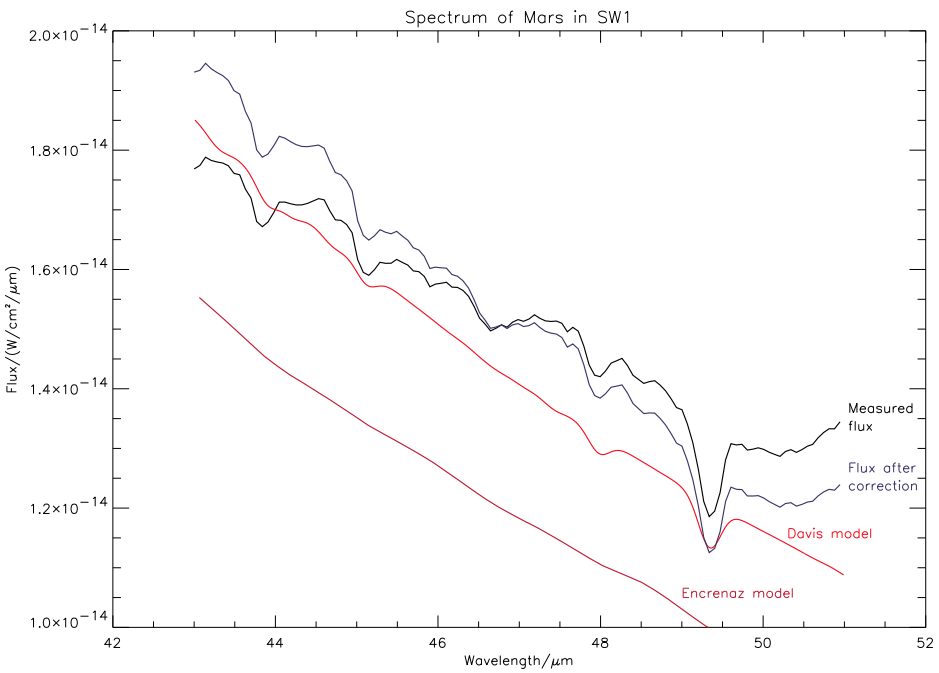

Figure 9: Comparison of theoretical Mars spectra with the observation for detector SW1

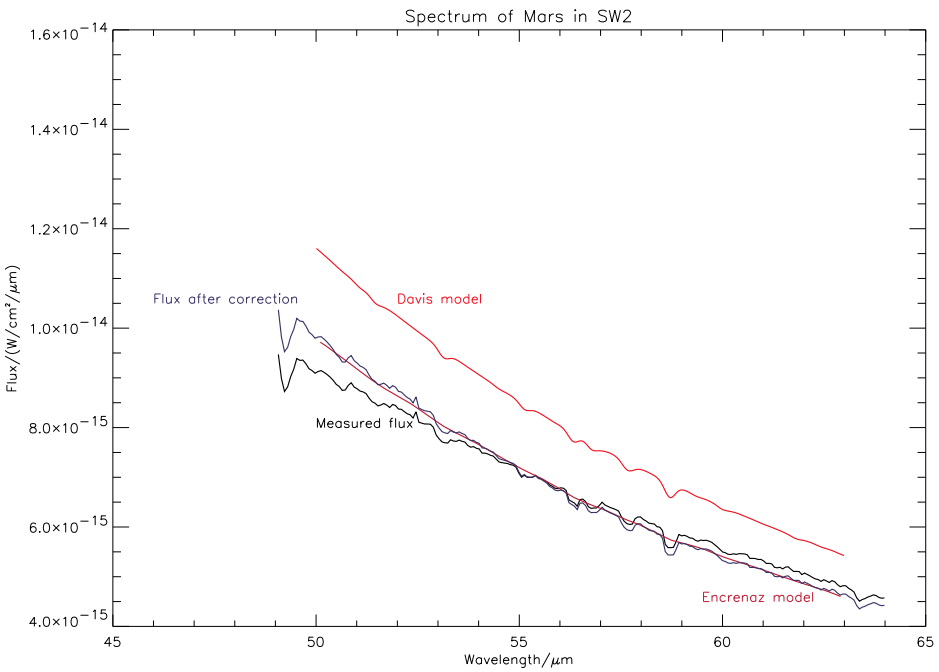

Figure 10: Comparison of theoretical Mars spectra with the observation for detector SW2

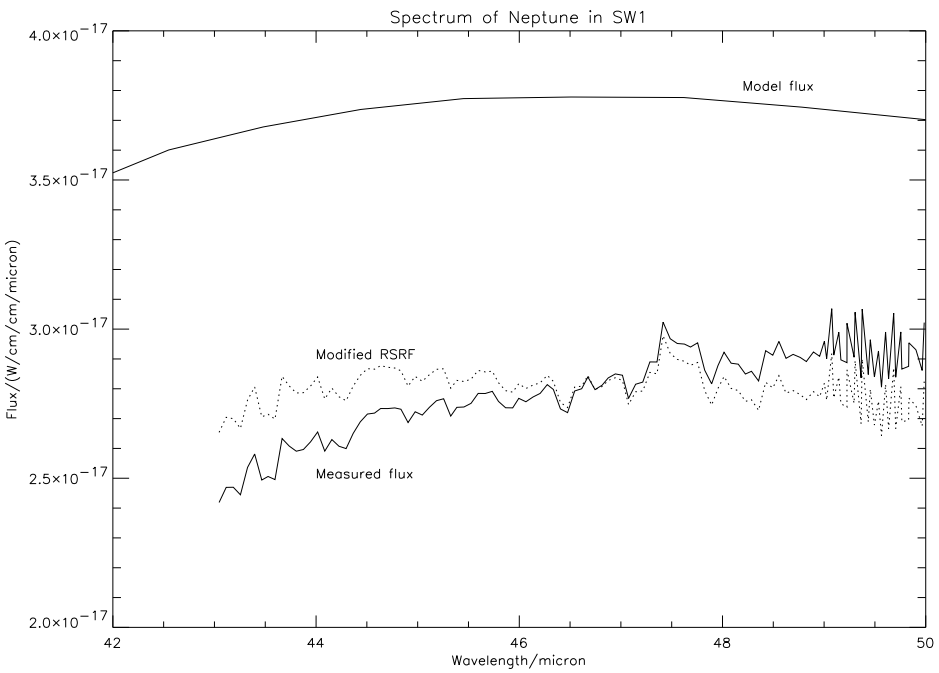

Figure 11: Comparison of the model spectrum of Neptune in detector SW1 with the observation

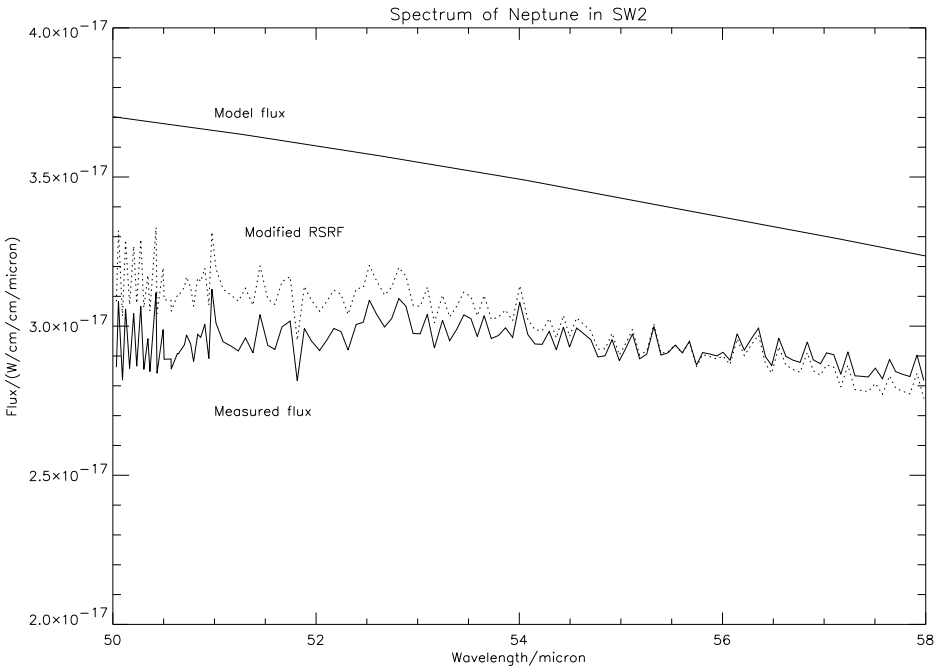

Figure 12: Comparison of the model spectrum of Neptune in detector SW2 with the observation

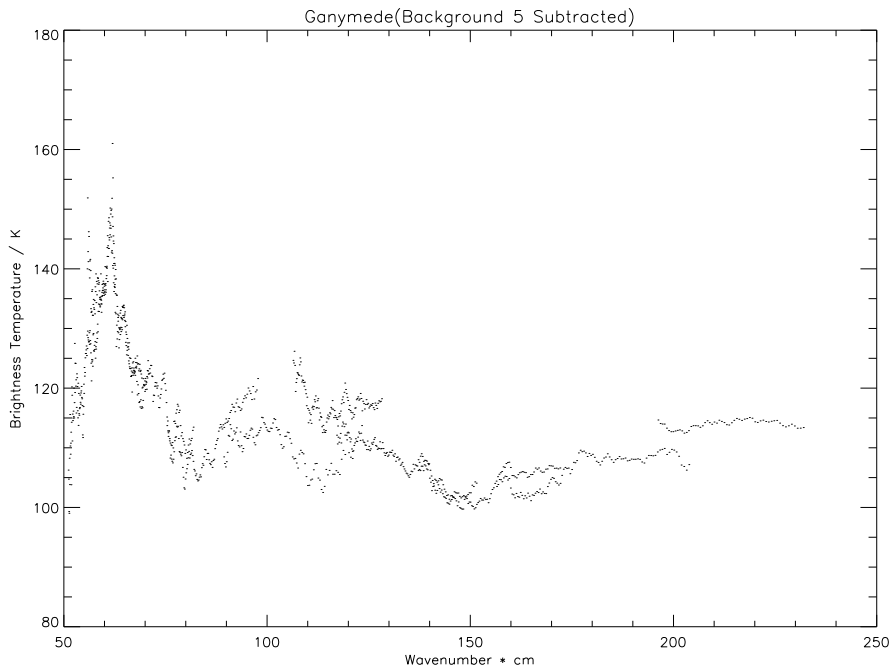

Figure 13: Spectrum of Ganymede as measured with the LWS (background subtracted)

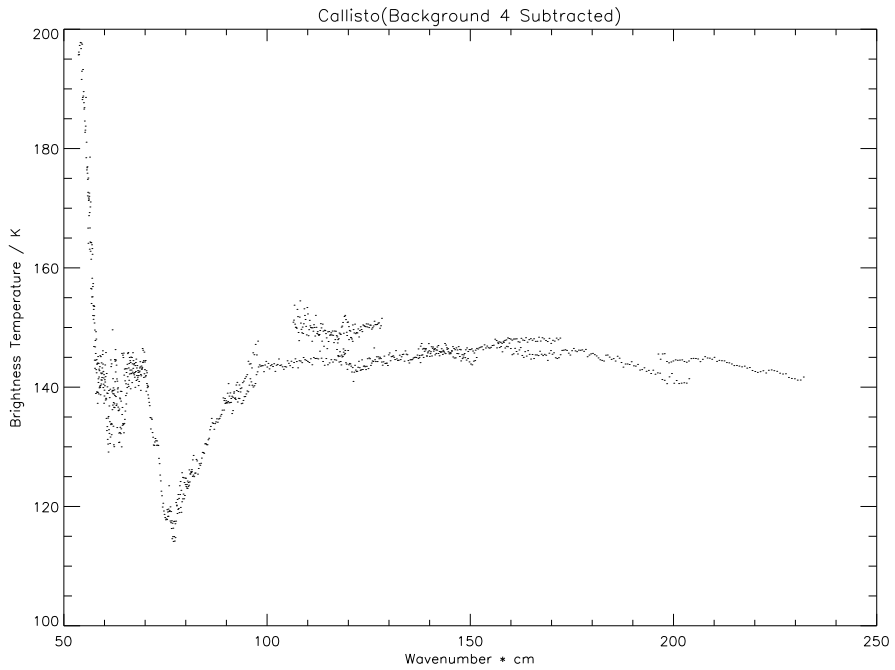

Figure 14: Spectrum of Callisto as measured with the LWS (background subtracted)

3 Appendix I - Routines Used

3.1 Routines Used to Monitor Galactic Sources

3.1.1 - List of Data Files

Input Files - For each object there is an input file nominally called scaninput.dat but for archiving purposes renamed to the object name eg S106input.dat. These contain the list of TDT numbers of all observations with L01 of the object.

Average Files - For each object there is a file containing a list of the revolution number and averages accross each of the ten detectors for each observation. The nominal name for this file is av_input.dat but for archiving purposes has been renamed to the object name eg S106.dat.

3.1.2 - Plotting Flux From Auto Analysis with Revolution

The scans are averaged per detector and an average across the whole detector is found for every observation.

1. The starting point is an input file eg s106input.dat, run the software this must be renamed to scaninput.dat.

2. The routine MAKE_AV.PRO is called from the IDL command line. It will ask "Are you doing this for the first time". If you wish to average the whole data set in arc_dat then 'y' or 'Y' should be entered. The 'N' or 'n' option was for updates following incoming weekly monitoring observations.

3. The output of MAKE_AV.PRO is the data file av_input.dat. MAKE_AV.PRO calls the averaging routine AVG_REBIN_MED.PRO.

4. In order to plot this data call TIMEWALK.PRO, this will look for a file called av_input.dat therefore in order to run this with the archived data files the object.dat file must be renamed to av_input.dat.

3.2 User note for the NEW-LCSI procedure for illuminator flash comparison

```
Outline:

The program NEW_LCSI takes the data from an illuminator flash processed
via CPD and compares to another similarly processed illuminator taken to be a
"standard".  The output is the form of a ratio and error between the
responsivity of each detector at the time the input illuminator was taken
compared to that at the time the "standard" illuminator flash was taken.

Use:

IDL>new_lcsi,stnam,lev=lev,fname=fname,ostat,dsig,bsig,odat,tfst,
dark=dark,data=data

where the inputs and outputs are:
INPUTS:   STNAM - name of MC_FITS LCPD file containing reference flash
```

```
optional  LEV   - illuminator level to search for
                  optional command line else prompted with STR_QUERY
          FNAME - name of MC_FITS LCPD file containing flash to be compared
                  optional command line else prompted with STR_QUERY
          DARK  - FLTARR(10) optional input dark currents else calculated
                  from data
          DATA  - optional input LCPD structure of illuminator flash to be
                  compared

OUTPUTS:  OSTAT - illuminator status lonarr(5)
           DSIG - corresponding detector signal fltarr(10,5)
           BSIG - FLTARR(2,10) background and error for each detector
           ODAT - FLTARR(10,2) - ratio and error for each detector
           TFST - average time (ITK seconds) for the flash

So at its most basic it can be used thus:

IDL>new_lcsi,'lcpd13304401',ostat,dsig,bsig,odat,tfst

where the file LCPD13304401 must in the ARC_DAT directory somewhere and
everything else will be prompted for.

Where is it:

The code is on COYOTE in [BMS.PROG]NEW_LCSI.PRO it requires the subroutine
ILLSTAT.PRO also found in [BMS.PROG] and some standard routines
from the CONMAN directories (MC stuff, STR_QUERY etc) these should be in your IDL
path if you're using a standard setup.

Any problems to Bruce Swinyard (BMS@SDC1.BNSC.RL.AC.UK).
```

4. Appendix II - Variation in Flux of Galactic Sources

SW1

Object	Mean before 377	Mean after 377	Sigma before 377	Sigma after 377	Sigma/Mean before 377	Sigma/Mean after 377
S 106	9.15E-16	7.76E-16	4.59E-17	1.91E-17	0.05	0.02
G 298	9.92E-16	8.31E-16	3.82E-17	1.84E-17	0.04	0.02
I23133		2.38E-16		6.01E-18		0.03
NGC 7027	1.19E-16	1.02E-16	8.46E-18	3.71E-18	0.07	0.04
NGC 6543	2.35E-17	2.17E-17	4.55E-18	1.69E-18	0.19	0.08

SW2

Object	Mean before 377	Mean after 377	Sigma before 377	Sigma after 377	Sigma/Mean before 377	Sigma/Mean after 377
S 106	8.67E-16	8.60E-16	2.25E-17	1.50E-17	0.03	0.02
G 298	8.65E-16	8.69E-16	1.85E-17	8.50E-18	0.02	0.01
I23133		2.67E-16		3.89E-18		0.01
NGC 7027	7.52E-17	7.45E-17	1.99E-18	1.97E-18	0.03	0.03
NGC 6543	1.55E-17	1.58E-17	8.01E-19	4.90E-19	0.05	0.03

SW3

Object	Mean before 377	Mean after 377	Sigma before 377	Sigma after 377	Sigma/Mean before 377	Sigma/Mean after 377
S 106	6.76E-16	6.75E-16	2.25E-17	1.35E-17	0.03	0.02
G 298	6.56E-16	6.57E-16	5.90E-18	7.39E-18	0.01	0.01
I23133		2.15E-16		1.50E-18		0.01
NGC 7027	4.93E-17	4.82E-17	1.79E-18	6.71E-19	0.04	0.01
NGC 6543	8.59E-18	8.77E-18	3.59E-19	2.20E-19	0.04	0.03

SW4

Object	Mean before 377	Mean after 377	Sigma before 377	Sigma after 377	Sigma/Mean before 377	Sigma/Mean after 377
S 106	5.05E-16	5.08E-16	1.85E-17	1.06E-17	0.04	0.02
G 298	4.76E-16	4.82E-16	6.86E-18	5.57E-18	0.01	0.01
I23133		1.71E-16		2.33E-18		0.01
NGC 7027	2.70E-17	2.78E-17	8.97E-19	2.87E-19	0.03	0.01
NGC 6543	4.80E-18	4.95E-18	2.61E-19	1.56E-19	0.05	0.03

SW5

Object	Mean before 377	Mean after 377	Sigma before 377	Sigma after 377	Sigma/Mean before 377	Sigma/Mean after 377
S 106	3.72E-16	3.68E-16	4.16E-18	4.03E-18	0.01	0.01
G 298	3.51E-16	3.52E-16	3.94E-18	4.00E-18	0.01	0.01
I23133		1.31E-16		6.47E-18		0.05
NGC 7027	1.82E-17	1.84E-17	6.60E-19	4.97E-19	0.04	0.03
NGC 6543	4.34E-18	4.30E-18	3.33E-19	2.37E-19	0.08	0.06

LW1

Object	Mean before 377	Mean after 377	Sigma before 377	Sigma after 377	Sigma/Mean before 377	Sigma/Mean after 377
S 106	2.08E-16	2.05E-16	6.48E-18	4.41E-18	0.03	0.02
G 298	1.87E-16	1.88E-16	2.84E-18	2.64E-18	0.02	0.01
I23133		8.10E-17		1.51E-18		0.02
NGC 7027	9.35E-18	9.41E-18	4.85E-19	2.10E-19	0.05	0.02
NGC 6543	2.22E-18	2.28E-18	1.71E-19	1.11E-19	0.08	0.05

LW2

Object	Mean before 377	Mean after 377	Sigma before 377	Sigma after 377	Sigma/Mean before 377	Sigma/Mean after 377
S 106	1.25E-16	1.16E-16	4.34E-18	2.67E-18	0.03	0.02
G 298	1.08E-16	1.04E-16	3.01E-18	1.70E-18	0.03	0.02
I23133		5.06E-17		7.65E-19		0.02
NGC 7027	4.47E-18	4.19E-18	2.65E-19	1.14E-19	0.06	0.03
NGC 6543	6.04E-19	6.49E-19	3.43E-20	2.44E-20	0.06	0.04

LW3

Object	Mean before 377	Mean after 377	Sigma before 377	Sigma after 377	Sigma/Mean before 377	Sigma/Mean after 377
S 106	6.98E-17	6.53E-17	3.60E-18	1.40E-19	0.05	0.02
G 298	5.71E-17	5.83E-17	1.31E-18	2.26E-18	0.02	0.04
I23133		3.14E-17		7.20E-19		0.02
NGC 7027	2.37E-18	2.38E-18	2.73E-19	7.39E-20	0.11	0.03
NGC 6543	2.80E-19	3.05E-19	1.90E-20	2.28E-20	0.07	0.07

LW4

Object	Mean before 377	Mean after 377	Sigma before 377	Sigma after 377	Sigma/Mean before 377	Sigma/Mean after 377
S 106	4.36E-17	4.16E-17	2.31E-18	1.04E-18	0.05	0.02
G 298	3.54E-17	3.67E-17	2.03E-18	7.51E-19	0.06	0.02
I23133		2.04E-17		3.85E-19		0.02
NGC 7027	1.48E-18	1.48E-18	1.76E-19	7.10E-20	0.12	0.05
NGC 6543	1.66E-19	1.92E-19	2.25E-20	3.08E-20	0.14	0.16

LW5

Object	Mean before 377	Mean after 377	Sigma before 377	Sigma after 377	Sigma/Mean before 377	Sigma/Mean after 377
S 106	3.35E-17	2.98E-17	3.17E-18	7.18E-19	0.09	0.02
G 298	2.62E-17	2.57E-17	3.08E-19	4.08E-19	0.01	0.02
I23133		1.46E-17		3.00E-19		0.02
NGC 7027	1.06E-18	9.63E-19	3.74E-19	5.19E-20	0.35	0.05
NGC 6543	1.65E-19	1.94E-19	5.76E-20	4.67E-20	0.35	0.24